Development of Front End Electronics for the Q_{weak} Drift Chambers

A thesis submitted in partial fulfillment of the requirements
for the degree of Bachelor of Science with Honors in
Physics from the College of William and Mary in Virginia,

by

Graham K. Giovanetti

Accepted for _____
(Honors)

_____
Advisor: Dr. Keith Griffioen

_____
Advisor: Dr. Klaus Grimm

_____
Dr. John Delos

_____
Dr. William Kossler

_____
Dr. Virginia Torczon

Williamsburg, Virginia
May 2006

Abstract

The Q_{weak} experiment at Jefferson Lab will carry out a precision measurement of the proton's weak charge, Q_W^p, by measuring elastic parity-violating asymmetries in electron-proton scattering. Variation from the Standard Model's prediction of Q_W^p may indicate new physics. An integral part of the Q_{weak} experimental apparatus is a vertical drift chamber being constructed in a clean room at The College of William and Mary. This thesis aims to develop a set of prototype front-end electronics for use with the drift chamber.

Acknowledgements

Thanks to Dr. Klaus Grimm and Dr. Keith Griffioen for their guidance and support.

Contents

1 Introduction

In 1927 Wigner [1] developed the concept of parity conservation, the idea that particle interactions would behave identically under a spatial inversion. For many years physicists believed that the conservation of parity, much like conservation of energy or momentum, was a fundamental law of nature. In 1956 Lee & Yang [2] found indications while observing pionic decay that, unlike the electromagnetic and strong forces, the weak force violated parity. After studying previous work on fundamental forces Lee & Yang came to the conclusion that although experiments on the strong and electromagnetic force showed convincing evidence for parity conservation, experiments on the weak force showed no evidence for parity conservation. Their work led Madame Wu and collaborators [3] in 1957 to study the $\beta-$ decay of ^{60}Co nuclei . Cobalt can be polarized when its thermal disorder is small enough to be overcome by the magnetic moment of the cobalt atoms. Wu accomplished the polarization of the ^{60}Co by placing it in a solenoid and cooling it to .01K. She then observed the electrons emitted during β decay of the ^{60}Co into ^{60}Ni and noticed an asymmetry in their momentum. This discovery showed that the weak force, the force responsible for β decay, was parity violating.

Innovations in the description of the weak force occurred during the 1960s when Glashow, Salam, and Weinberg [4] developed the unified electroweak theory combining the electromagnetic and weak forces. This theory had several predictions, including the existence of three previously unimagined bosons. In 1983 physicists at CERN near Geneva Switzerland [1] detected all three of these bosons, W^+ W^- and Z^0, in an experiment involving the collision of a proton and an antiproton beam. This helped to further support the unified electroweak theory which is now universally incorporated into the Standard Model.

The electroweak theory makes a firm prediction of the weak charge of the proton. The Q_{weak} experiment at Jefferson Lab will carry out a precise measurement

of the proton's weak charge, Q_W^p, by measuring elastic parity-violating asymmetries in electron proton scattering. The measurement will take place at a very low four-momentum transfer squared, $Q^2 = 0.03\text{GeV}^2$, and at forward angles. The resulting measurement of Q_W^p will be one the first high-precision measurements of the weak force of the proton. Deviation from the electroweak model's prediction may be a sign of new physics, whereas agreement further supports the Standard Model.

2 The Physics of Q_{weak}

2.1 The Weak Force and Parity Violation

The weak force, one of the three fundamental forces described in the Standard Model, is the only force that violates parity conservation. The weak force is carried by W^+, W^-, and Z^0 bosons. The W^+ boson can only interact with right handed fermions and the W^- boson can only interact with left handed fermions. The Z^0 couples to left and right handed fermions, but with different magnitudes

$$M_{LH}^{Z0} \neq M_{RH}^{Z0} \tag{1}$$

The weak interaction is responsible for the transformation of leptons or quarks from one flavor to another. It is most commonly seen in $\beta-$ decay, in which one of the down quarks in a neutron emits a W boson and becomes an up quark, this W boson then decays into an electron and a neutrino.

A parity transformation is the flip of all spatial coordinates in a system. Initially physicists believed parity transformations left fundamental physical interactions unchanged. Interactions observed to that point, such as gravity, were dependent on distance alone, and therefore an inversion of all spatial coordinates didn't modify the interaction. In 1957 the $\beta-$ decay experiment performed by Madame Chien-Shiung Wu showed that the weak force is parity violating.

In the Q_{weak} experiment the weak force manifests itself as the difference in the number of right handed, σ_+, and left handed, σ_-, elastically scattered electrons from an unpolarized proton target. The asymmetry, A_{LR}, is defined as the cross sectional difference between left-handed and right-handed polarized electrons divided by their sum.

$$A_{LR} = \frac{\sigma_+ - \sigma_-}{\sigma_+ + \sigma_-} \tag{2}$$

This asymmetry is the sum of a term proportional to the weak charge of the proton, Q^P_{weak} and a term dependent on the strong interaction:

$$A_{LR} \propto Q^2 Q^P_{weak} + A_s Q^4 \tag{3}$$

When momentum transfer is low, such as in the Q_{weak} experiment where Q^2 is precisely defined as 0.03 $(\mathrm{GeV})^2$, the effects of the strong force are minimized, leaving the asymmetry proportional to the weak charge of the proton. Using A_{LR} one can then determine the weak mixing angle, also known as the Weinberg angle, through the relationship:

$$Q^P_W = 1 - 4\sin^2\theta_W \tag{4}$$

The measured Weinberg angle can then be compared to the Standard Model's predictions.

2.2 Four-momentum Transfer Squared, Q^2

The Q_{weak} experiment is unique in that it aims to take a measurement of the weak charge of the proton at low Q^2 where contributions from the internal structure of the proton are relatively small. This greatly simplifies the interaction and minimizes uncertainties inherent at higher Q^2. In order to obtain good results for the weak charge of the proton in this experiment (equation 4) it is important to precisely know the Q^2 of the detected elastically scattered electrons. Q^2 is defined as $Q^2 \equiv -q^2$ where $-q$ is the four-vector of the electron-proton interaction. We can then write q^2

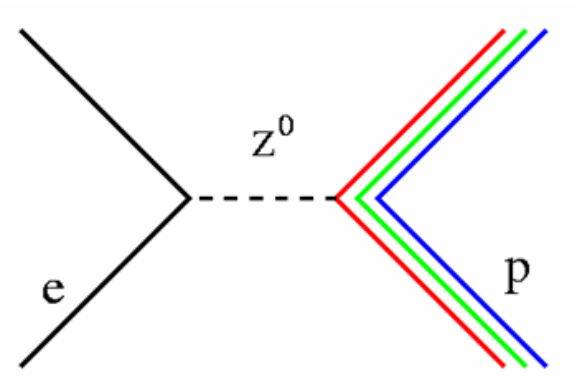

Figure 1: The weak interaction, carried by the Z^0 boson, in electron-proton scattering.

as the squared norm of a four-vector.

$$q^2 \equiv q_\mu q^\mu = (p_\mu - p'_\mu)(p^\mu - p'^\mu) \tag{5}$$

$$= p_\mu \cdot p^\mu - p_\mu \cdot p'^\mu - p'_\mu \cdot p^\mu + p'_\mu \cdot p'^\mu \tag{6}$$

$$\tag{7}$$

where p_μ is the initial four-momentum of the electron and p'_μ is the four-momentum of the electron after scattering. We determine the dot products:

$$p_\mu \cdot p^\mu = \left(E, \vec{p}\right)\begin{pmatrix} E \\ -\vec{p} \end{pmatrix} = EE - \vec{p} \cdot \vec{p} \tag{8}$$

$$p'_\mu \cdot p'^\mu = \left(E', \vec{p'}\right)\begin{pmatrix} E' \\ -\vec{p'} \end{pmatrix} = E'E' - \vec{p'} \cdot \vec{p'} \tag{9}$$

$$p_\mu \cdot p'^\mu = \left(E, \vec{p}\right)\begin{pmatrix} E' \\ -\vec{p'} \end{pmatrix} = EE' - \vec{p} \cdot \vec{p'} \tag{10}$$

$$p'_\mu \cdot p^\mu = \left(E', \vec{p'}\right)\begin{pmatrix} E \\ -\vec{p} \end{pmatrix} = E'E - \vec{p'} \cdot \vec{p} \tag{11}$$

and can then write

$$q^2 = (E^2 - p^2) - 2(EE' - \vec{p} \cdot \vec{p'}) + (E'^2 - p'^2) \tag{12}$$

We know the energy of a particle to be $E^2 = m^2 + p^2$. In the case of a high energy

particle experiment $m^2 \ll p^2$, making $E \approx p$. Using this information we find

$$q^2 = -2EE'(1 - \cos\theta) \tag{13}$$

Since $1 - \cos\theta = 2\sin^2\left(\frac{\theta}{2}\right)$ we can write

$$Q^2 = 4EE'\sin^2\left(\frac{\theta}{2}\right) \tag{14}$$

During construction it is necessary to know the scattering angle of electrons with a specific Q^2 so that the apparatus may mechanically select the correct electrons. During the calibration stage of the experiment the average Q^2 of detected electrons is determined using data collected from the tracking system. This is necessary for an accurate determination of Q_W^p.

2.3 The Standard Model

The Standard Model makes a firm prediction of the change in the weak mixing angle with increasing Q^2. This is known as the running of $\sin^2\theta_W$. In order to test the validity of the predicted running of $\sin^2\theta_W$ there must be a set of precise measurements at various Q^2 values. To date there have been very high precision measurements of $\sin^2\theta_W$ near the Z^0 pole but very few at lower Q^2 [5]. The Q_{weak} experiment aims to make a measurement of $\sin^2\theta_W$ well below the Z^0 pole in order to understand the running of $\sin^2\theta_W$. Other measurements come from atomic parity violation (APV), high energy neutrino-nucleus scattering (NuTev), and the E-158 experiment at SLAC [5]. All of these experiment have large systematic and statistical errors (fig. 2). The Q_{weak} measurement will have unprecedented precision due to its simplicity and our good understanding of the proton's structure.

The Standard Model has been very successful in describing existing experimental data. However, there are reasons to believe that it is not a complete description of fundamental physics, especially at higher energy scales. Many parameters, such as masses, mixing angles, and couplings, must be determined experimentally and added

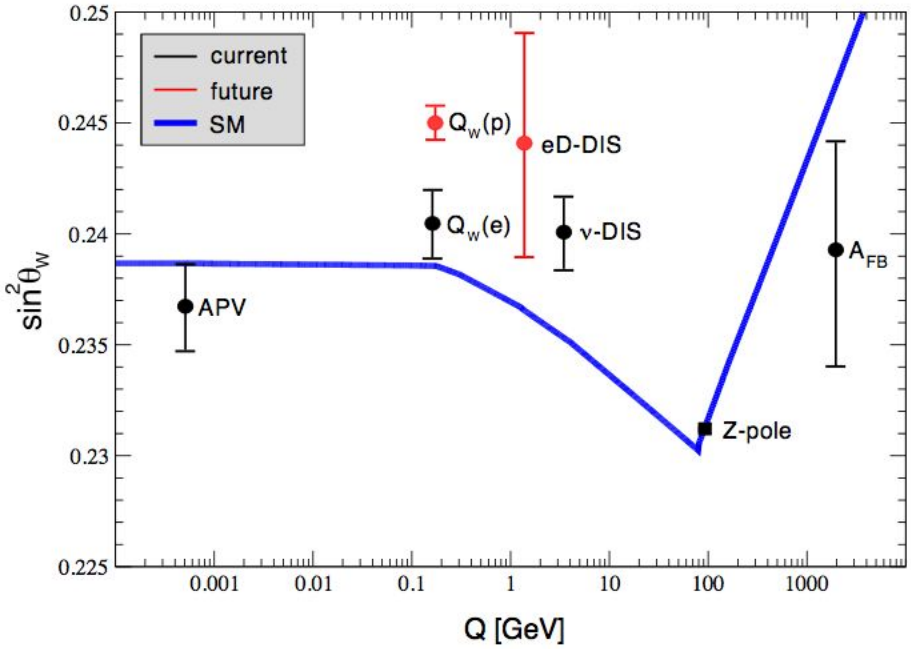

Figure 2: The calculated running of the weak mixing angle in the Standard Model. The black error bars show current experimental data. The red error bars show future experiments, including Q_{weak}, with an arbitrary vertical location.

ad hoc into the theory. Other observed phenomena, such as parity violation, are not explained by the theory but only incorporated into it. One might expect a complete theory to provide deeper insight into such phenomena. A possible experimental deviation from the Standard Model was published in 1998 by the Super-Kamiokande observatory [1] which observed neutrino oscillations. Measurements of $\sin^2\theta_W$ that deviate from the Standard Model's prediction may also be an indication of physics beyond the Standard Model.

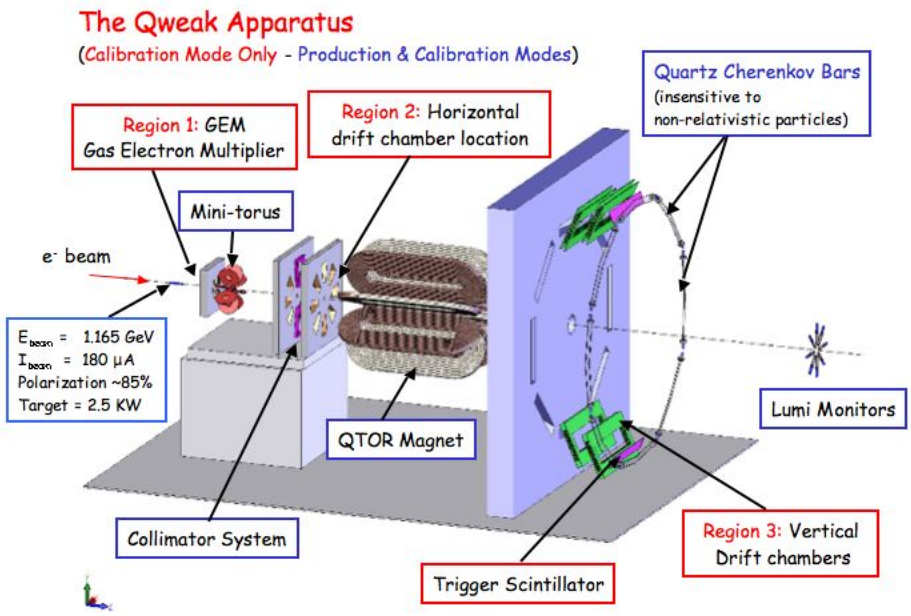

Figure 3: The Q_{weak} apparatus.

3 Experimental Apparatus

Over twenty institutions are involved in the design and construction of the Q_{weak} experiment [5]. The apparatus, created specifically for Q_{weak}, uniquely combines a high beam current with a low momentum transfer (Q^2). Installation of hardware in Hall C of Jefferson Lab is scheduled to begin in the end of 2008.

In order to determine Q_W^p, the Q_{weak} collaboration will make a 2200 hour measurement of the asymmetry in elastic electron-proton scattering. The experiment will use an 80% polarized 1.2GeV electron beam scattered from a 35 cm target of liquid hydrogen. Scattered electrons pass through precision machined collimators that select electrons with a scattering angle of 9 $\pm$2 degrees corresponding to the desired momentum transfer $Q^2 = .03$ GeV^2. These selected electrons then cross a magnetic field created by a large toroidal magnet (fig. 4). The magnetic field deflects any electrons with incorrect momentum and focuses the electrons with the desired momentum onto

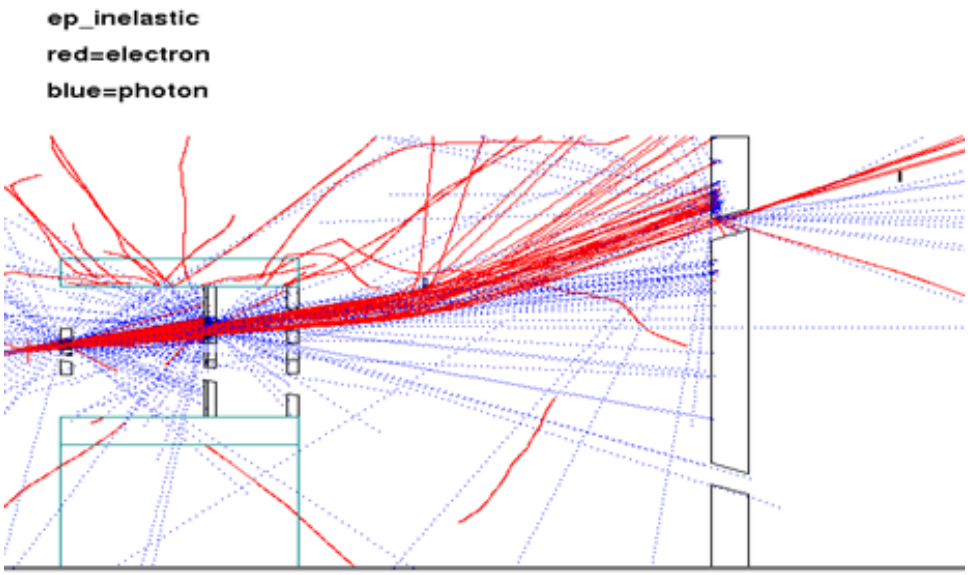

Figure 4: Simulation of inelastic electron-proton scattering events. A majority of inelastic events are filtered by the collimators in the left of the figure or their trajectory is changed by the magnetic field of the toroidal magnet such that they cannot pass through the shielding wall. Those inelastic events that do pass through the shielding wall don't hit the small black Cerenkov detectors in the right of the figure.

eight quartz Cerenkov detectors (fig. 5).

Quartz has an index of refraction $n \approx 1.4$, which corresponds to a speed of light in the medium of x% of the speed of light in a vacuum. As scattered electrons pass through the Cerenkov detector their electromagnetic field displaces electrons in the dielectric. When these electrons return to equilibrium they emit a photon. Typically these photons destructively interfere, however when the speed of the disrupting electromagnetic field is greater than the speed of light in the medium, xc, the photons constructively interfere and create a shock cone of light (much like the sonic boom created by a jet). This is called the Cerenkov effect. The emitted light is then detected by photomultiplier tubes attached to both ends of the Cerenkov detectors. The phototubes convert the light pulses into electrical signals. With such a high event rate

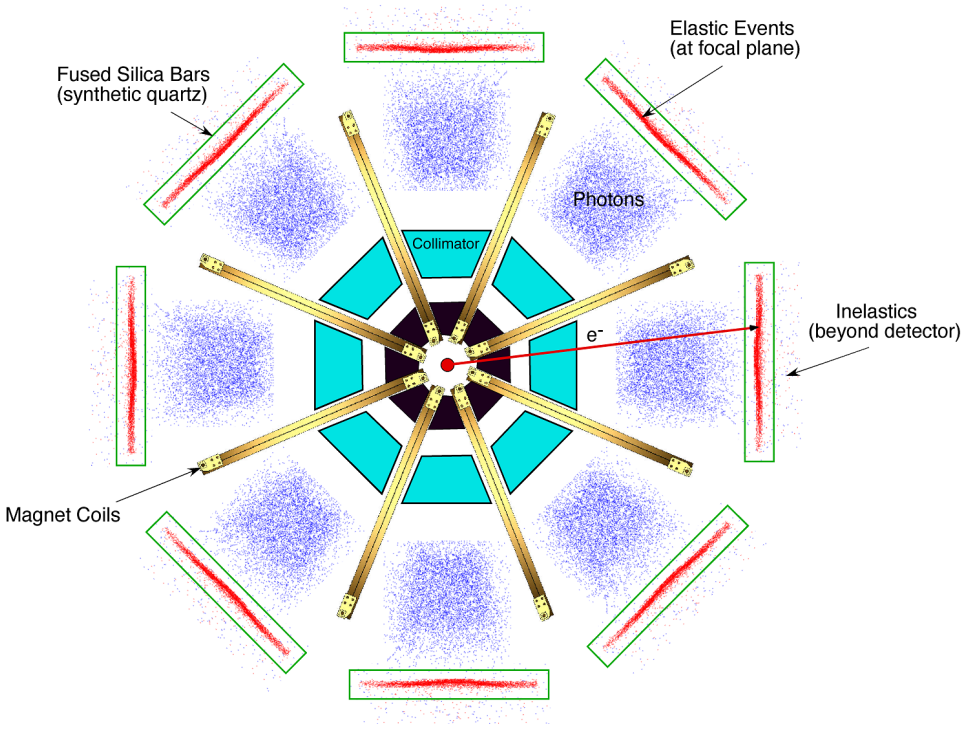

Figure 5: View of the Q_{weak} experiment down the beam line. Elastically scattered electrons strike the eight Cerenkov detectors arranged in a ring around the beam line. Notice scattered photons, in blue, and inelastic events do not strike the detectors

the signals are integrated rather then counted individually. In this way the number of electrons elastically scattered from the proton is determined (fig. 6). Cerenkov detectors have the advantage of eliminating potential background noise caused by low energy particles. The quartz Cerenkov detectors used in Q_{weak} are also radiation hard, meaning the quality of their optical transmission will not degrade from radiation over the course of the experiment.

3.1 The Tracking System

Prior to running the Q_{weak} experiment in data production mode, a tracking system will be employed to map the response of the Cerenkov detectors, determine the average Q^2 of elastically scattered electrons, and find the systematic error caused by

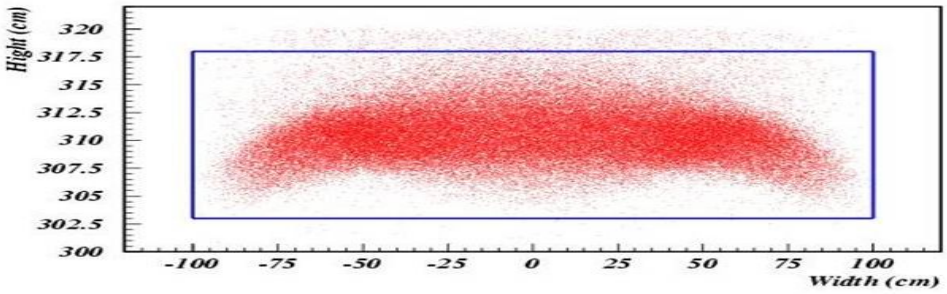

Figure 6: The simulated distribution of elastically scattered electrons events on the Cerenkov bars

inelastically scattered electrons striking the Cerenkov bars. This tracking system consists of a gas electron multiplier (GEM), a horizontal drift chamber (HDC), a set of vertical drift chambers (VDC), and a trigger scintillator which starts the data acquisition system. The GEM and HDC provide a reconstruction of the track of individually scattered electrons. This is used to determine their scattering angle. The VDCs determine the trajectory of electrons exiting the magnetic field of the toroidal magnet. With this trajectory and a precise knowledge of the magnetic field (found through simulation or through magnetic field mapping) the momentum of individual electrons can be determined. Combining the momentum of an electron with its scattering angle allows one to calculate Q^2 and separate elastically scattered electrons from inelastic events.

The tracking system cannot be used when the experiment is running in production mode because of the high event rate, about 800 MHz per octant. This is chiefly due to the large quantity of low energy Moller electrons from electron-electron scattering, which occurs at a rate 250 times that of electron-proton scattering, striking the HDC. In calibration mode the count rate is decreased by four orders of magnitude to 40 KHz per octant. At this event rate it is possible to track individual electrons for the purpose of establishing the number of inelastic events detected by the Cerenkov detectors as well as determine the average Q^2 of scattered electrons. Lastly one can determine the response of the Cerenkov detectors based on the location the electron

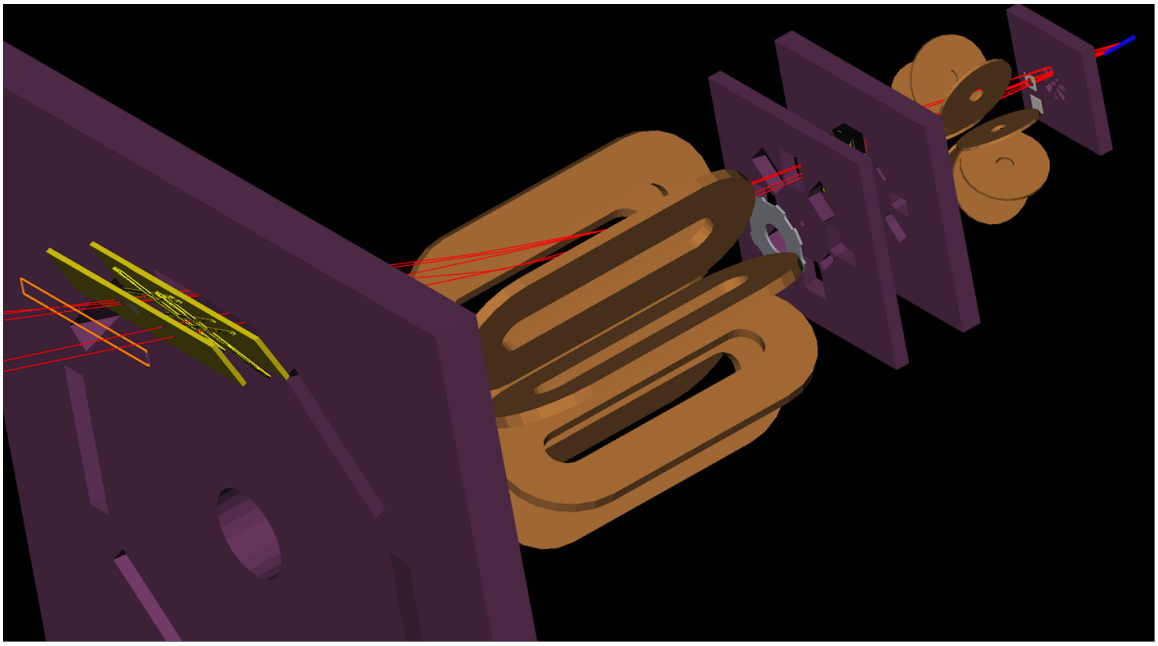

Figure 7: GEANT simulation of the Q_{weak} apparatus. The entire tracking system can be seen in this figure. In the right of the figure is the gas electron multiplier colored in purple. The purple devices to its left are the collimator and the horizontal drift chamber. Behind the large shielding wall, in the left of the figure, lie the vertical drift chambers (colored yellow) being constructed at William & Mary

strikes them.

3.2 Drift Chambers

A crucial element of the tracking system for Q_{weak} are the drift chambers. These are used to determine the trajectory of any charged particles that pass through it. A drift chamber consists of a cavity filled with an easily ionizable gas and a matrix of wires. Charged particles entering the chamber collide with gas molecules. If enough energy is transferred in this collision an electron-ion pair is produced. Due to an applied voltage across the chamber these freed electrons drift towards the closest wire (fig. 8). Far from the wires the velocity of the drifting electron remains fairly constant.

Close to a wire the electron accelerates rapidly, ionizing gas molecules in its path. This creates more electron-ion pairs whose electrons in turn collide with other gas molecules and ionize them. This repeating process is known as the avalanche effect and is measured as a charge on the wire (fig. 10).

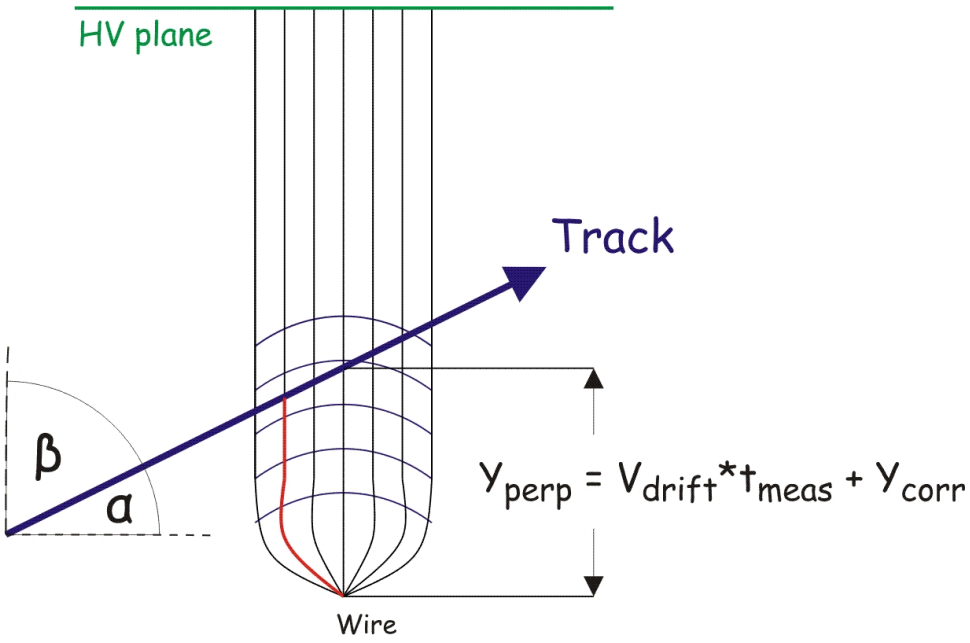

Figure 8: Electric field lines for a wire in the drift chamber. The y_{perp} distance is the measured distance of a particle from the wire

A charged particle passing through the drift chamber will create a signal on several of the wires in the matrix (fig. 9). By recording the time of these "hits" one can accurately recreate the path the particle took through the chamber. The transformation used to extract the particles position based on signal timing is determined using a computer simulation.

Planar drift chambers come in two configurations known as horizontal and vertical drift chambers. The names follow from the direction that ionized electrons preferably travel in the chamber. A horizontal drift chamber consists of 6-8 planes of wires stacked together. Planes are arranged in different orientations. At least two planes per orientation are need to remove any ambiguity in the measurement. Each particle

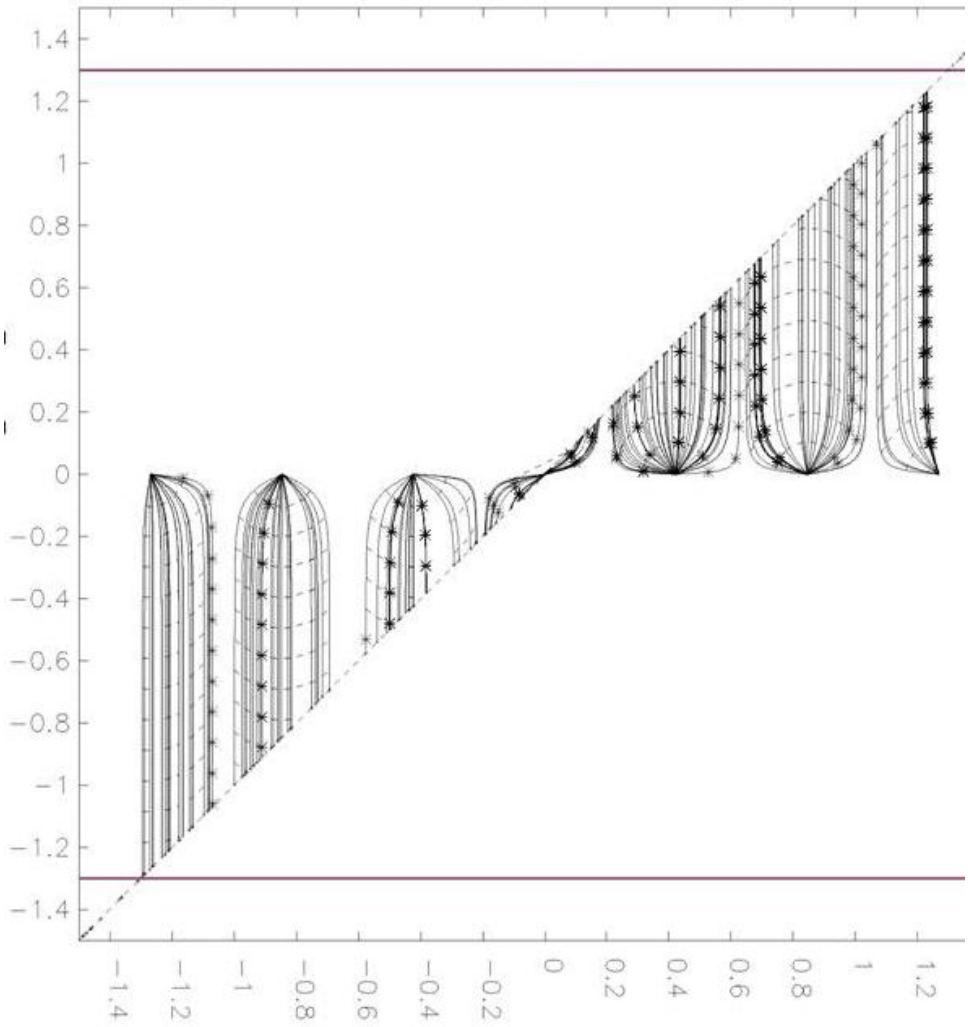

Figure 9: The track of an electron passing through the vertical drift chamber. Curved lines represent the track of free electrons drifting towards the wires, which are represented by points, along the x axis. The solid lines are the voltage planes on either side of the wire chamber carrying a negative voltage.

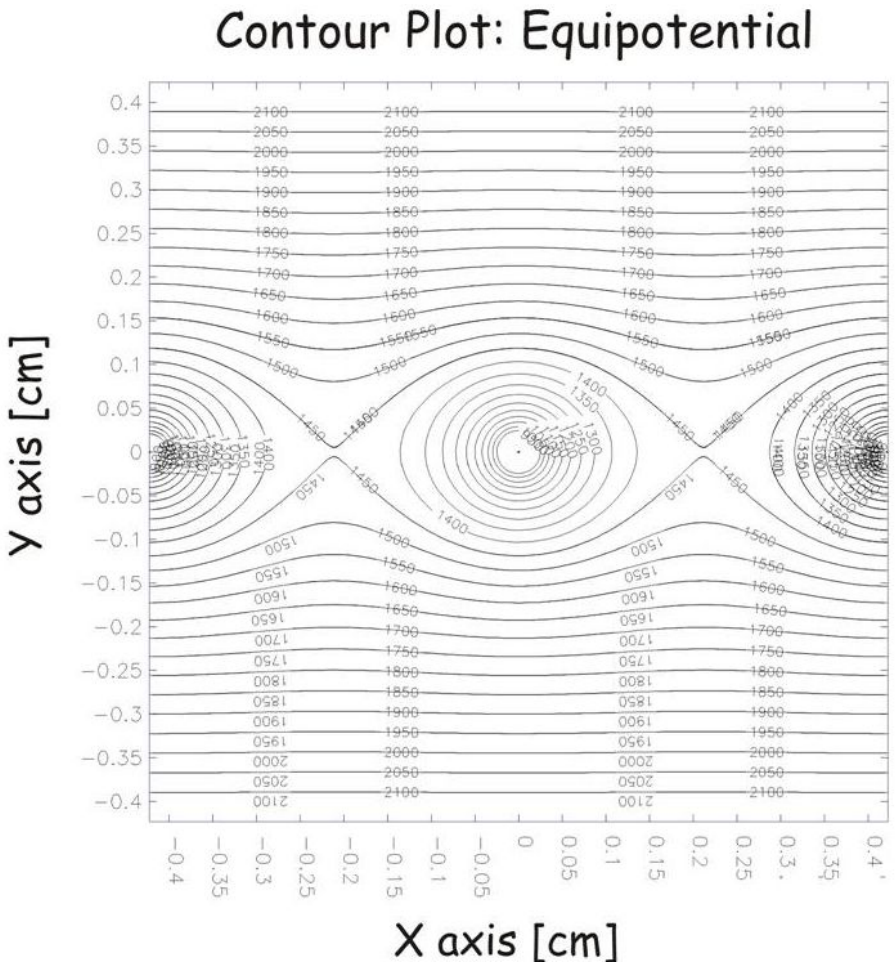

Figure 10: The equipotential at the wires in a drift chamber. The concentric circles close to the wire define the area where the avalanche effect occurs.

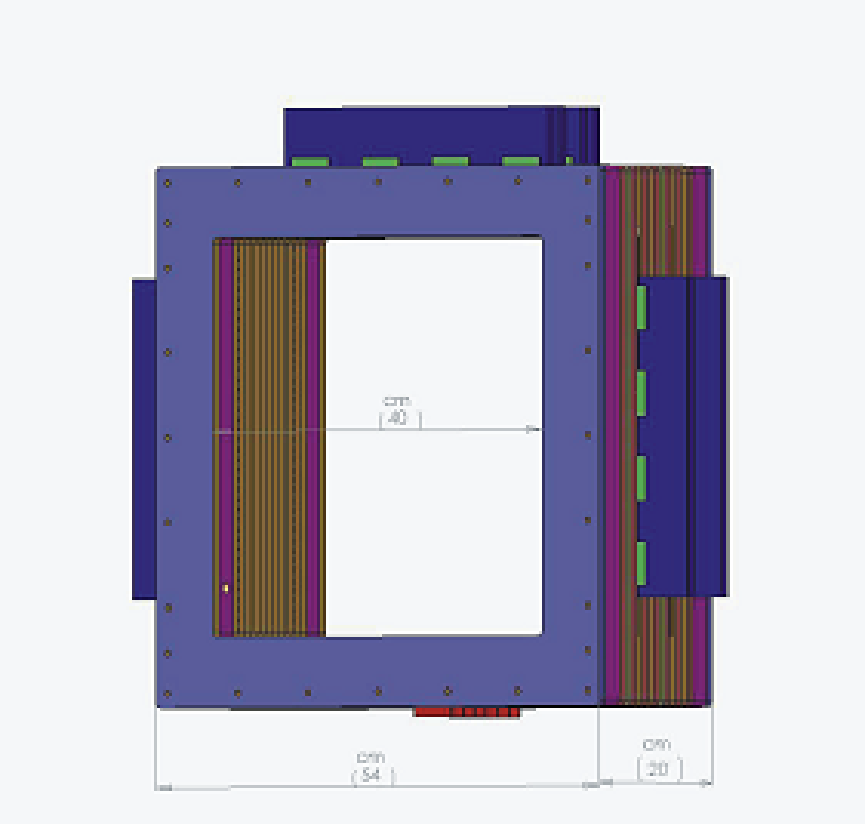

Figure 11: Horizontal drift chamber in the Q_{weak} experiment.

passing through a horizontal drift chamber will create a signal on only one wire per plane (fig. 11). Vertical wire chambers consist of only two planes of wires because particles passing through the chamber create 5-8 hits per plane. Vertical drift chambers have the advantage of a resolution almost twice that of horizontal drift chamber and a much simpler electric field within the chamber. However, vertical drift chambers have an acceptance angle of 10 degrees, much lower than a horizontal drift chamber which can accept particles over approximately a 60 degree angle.

The vertical drift chambers used in the Q_{weak} experiment will be constructed in a clean room at The College of William and Mary. These chambers consist of two wire planes, each strung with two sets of wires that cross each other at a 45^o angle (fig. 12). To prevent sagging of the wires in the chamber each wire is oriented at a 45^o angle to the frame. These drift chambers must be equipped with an electronics

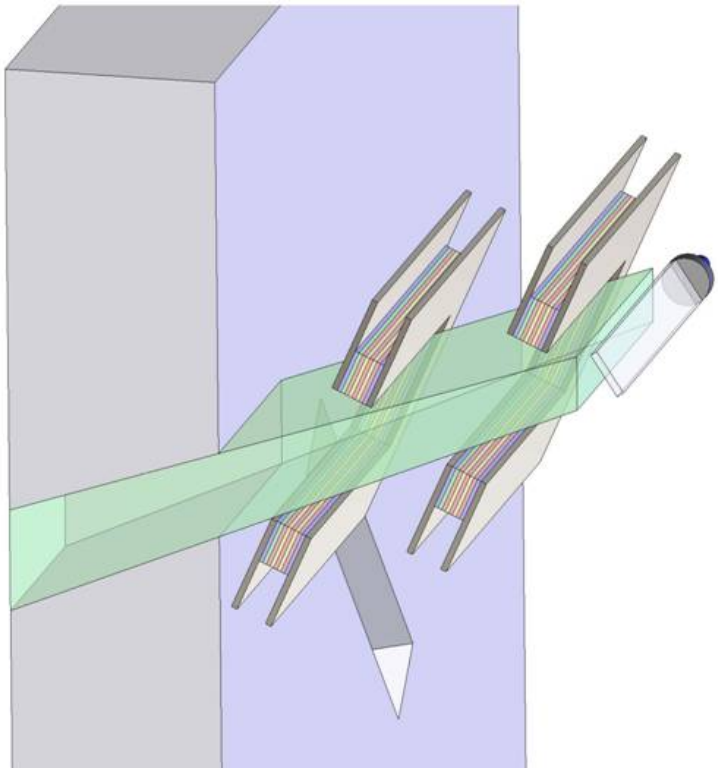

Figure 12: The vertical drift chambers of the Q_{weak} experiment.

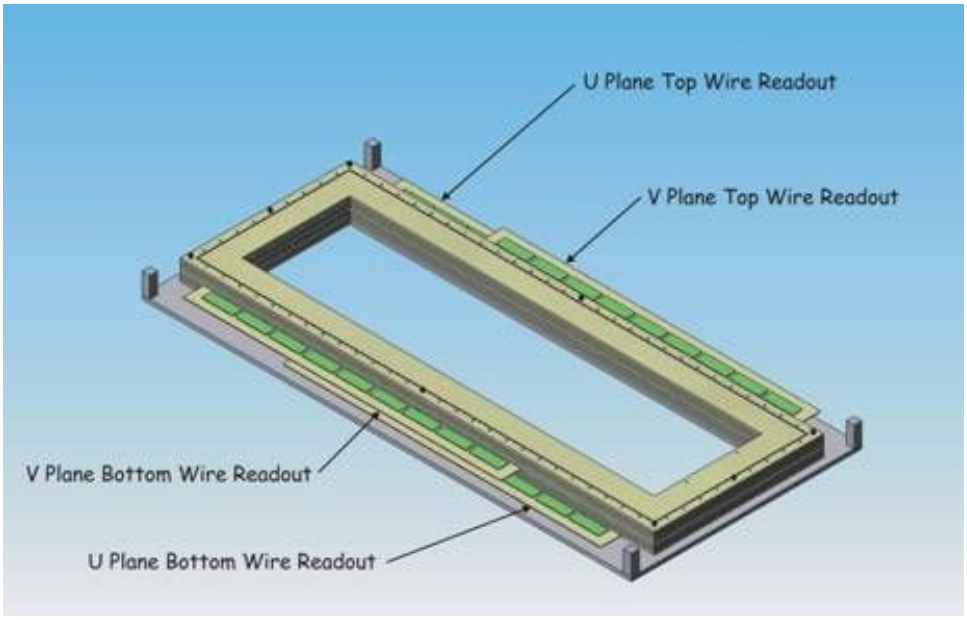

Figure 13: The frame used for the vertical drift chambers.

package to process signals from individual wires in the chamber.

3.3 The Multiple Amplifier Discriminator Chip

The multiple amplifier discriminator (MAD) chip is a four channel amplifier and discriminator designed in Padova, Italy to be used with drift chambers. The MAD chip serves as the centerpiece of the Q_{weak} vertical drift chamber's front-end electronics. Each channel of the MAD chip is attached to an individual wire of the drift chamber. When an electron passes through the chamber a negative voltage pulse is transmitted by the wire to the MAD chip. The pulse is on the order of a mV. This analog signal from the chamber first goes through a preamplifier and a shaper which superimposes the voltage pulse onto a quiescent level. The quiescent level, essentially the base level or reference voltage, of the shaper is set by a pin on the chip (VREF). The signal, now positive from a negative charge applied to the preamp and superimposed on the reference voltage, goes through a leading edge discriminator. The discriminator triggers at a threshold voltage set by pin VTH and produces a digital TTL signal.

The digital pulse then passes through a one-shot that lengthens the pulse in a manner inversely proportional to the current sunk from pin W_CTRL. Both W_CTRL and VTH are common to all four channels of the MAD chip. Finally, the signal proceeds through a differential voltage driver which produces a low voltage differential signal (LVDS), essentially a two line signal where one line carries the pulse and the other carries an inverted version of the pulse (fig. 14). By running these two lines in parallel one can eliminate much of the noise picked up when passing a signal any significant distance in an electrically noisy environment by simply taking the difference of the two wires at the end point. This wire pair also produces little external magnetic field that could influence other wires nearby. This influence is called cross talk. The MAD chip also takes internal precautions against crosstalk by designing the chip circuitry so that every channel is independent.

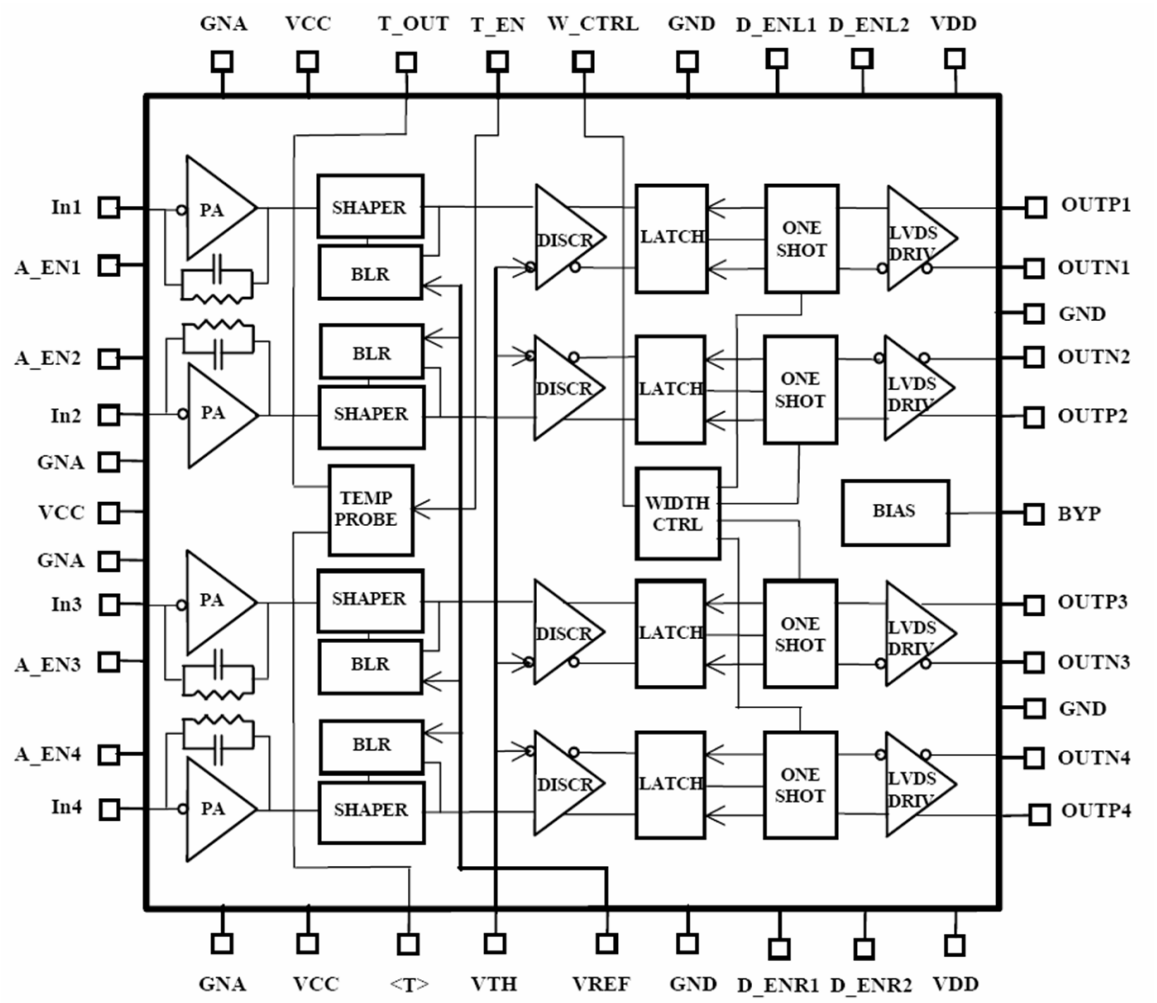

Figure 14: Pin inputs and internal electronics of the MAD chip [6].

Other features of the chip include both analog and digital channel enabling and disabling. The analog enable is accomplished simply through a TTL signal. The digital enable requires a differential signal but has a much faster response time, 30 ns compared to 10μs for the analog case. The chip also provides internal temperature monitoring. This is important since the analog portion of the chip's performance can vary with changing temperature. Power for the chip is provided by two different power supplies, V_{CC} for the input section of the chip and V_{DD} for the output section of the chip. Both power supplies have their own ground, GNA for the input and GND for the output. This separation of power supplies helps to minimize possible

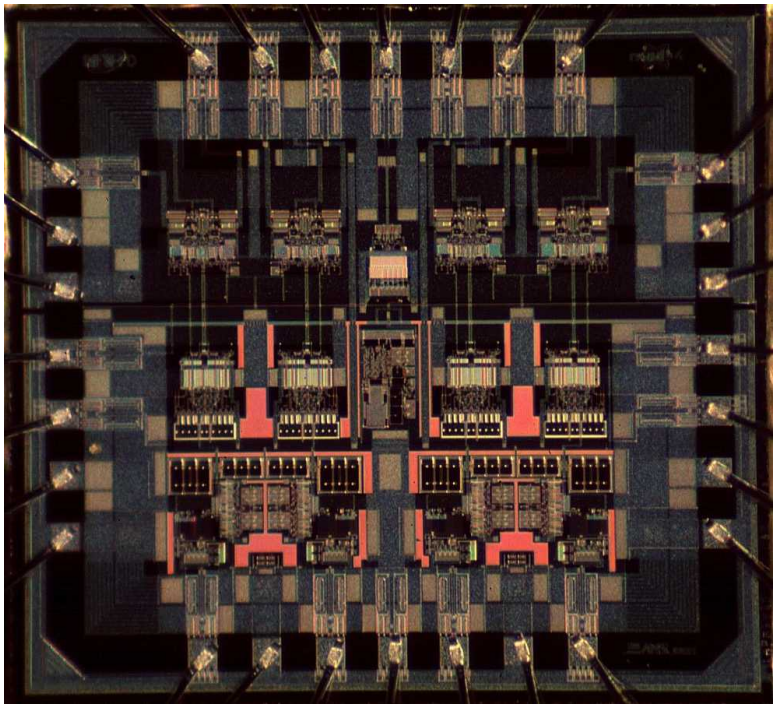

Figure 15: An internal view of the actual MAD chip [7].

interference in the chip. Over 600 mad chips were ordered for use in the vertical drift chambers (fig. 15).

4 Electronics

The vertical drift chambers being constructed at William and Mary must be instrumented with electronics to discriminate and amplify the voltage pulses on individual wires and also to monitor and control this process. I have worked to develop prototypes for several printed circuit boards (PCBs) for use with the drift chamber in different capacities. During testing of the drift chamber it is important to have the capability to turn on and off individual wire channels in the chamber in order to debug them. For this purpose I have developed a channel enable/disable board using an 8 channel I/O expander made by Phillips, the PCF8574. Another necessity is to read out the temperature of the MAD chips and surrounding circuitry. Much of this am-

plification and discrimination process is analog and can be affected by varying heat. The board developed as a prototype temperature monitor uses a chip from Dallas Semiconductor, the DS1631, capable of acting as a thermometer. In final designs the temperature will be read directly from the MAD chips. The channel enable/disable device and the thermometer device are controlled remotely using an I^2C serial bus developed by Phillips. The serial bus is controlled by attaching it to the printer port of a personal computer using an interface card we developed. This card also serves as the power supply for devices on the bus. I have also developed a board to test the MAD chip under various conditions to determine its characteristics and explore ways to get good timing information from input signals.

4.1 Eagle

In order to design these boards I have used the computer program Eagle, which is a layout editor produced by CadSoft for designing printed circuit boards. The program consists of three modules. The first step of PCB design is to use the schematic editor which allows one to lay out a schematic for a PCB using parts from either the extensive part libraries included in the Eagle package or ones designed by the user (fig. 16). After a schematic of the board is complete, the user turns it into a board layout using the layout editor module of the program (fig. 17). The board is then routed manually or by using the auto-router module that automatically routes the board based on specifications determined by the user. After routing and finalizing the PCB layout the board is converted into Gerber files. Gerber files are the format typically used by PCB houses in the fabrication of boards. These files contain all the information needed to mill the board, drill the appropriate holes, lay the solder mask and solder plating, and print the silk screening.

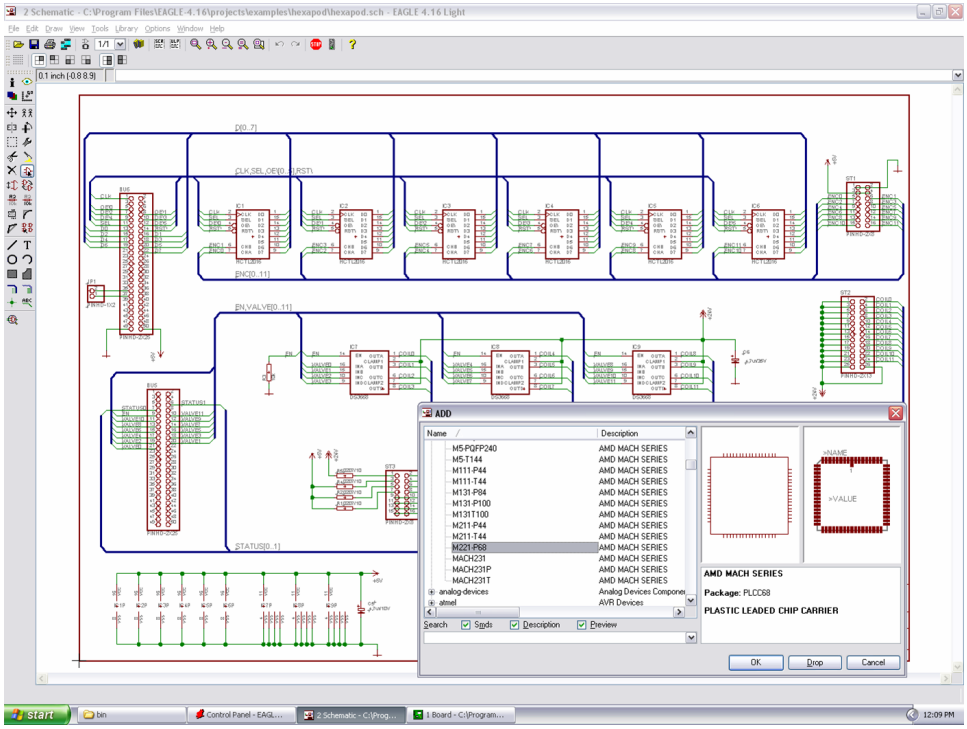

Figure 16: The schematic editor module in EAGLE.

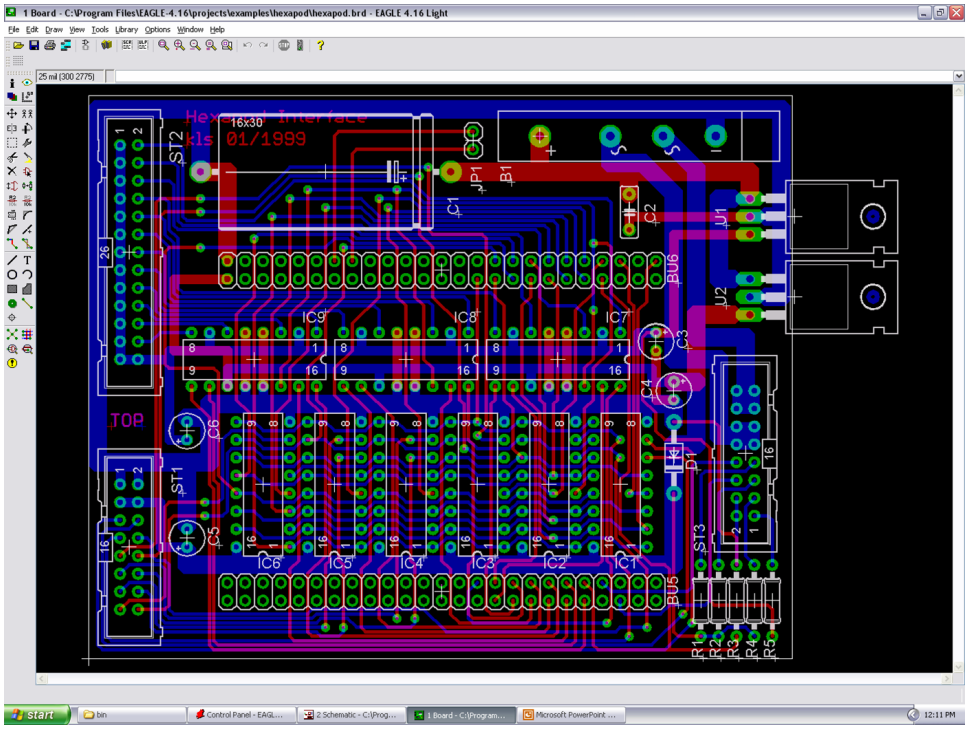

Figure 17: The board editor module in Eagle.

4.2 I^2C

All prototype PCBs will be controlled using I^2C, a serial bus developed by Phillips in the 1980s for use with low speed devices. A serial bus consists of a master device, in this case the computer, that controls slave devices attached to the bus. Linux has a built-in kernel module to handle the I^2C bus enabling control of devices with relatively simple computer code. The I^2C bus consists of two lines, the serial clock line (SCL) and the serial data line (SDA).

The I^2C protocol is as follows. The master device transmits a start signal to all devices on the bus (fig. 18). This signal alerts all slave devices to listen to the master device. After the start signal the master sends out a control byte consisting of a 7-bit address and a 1-bit read or write command. Every device on the bus has its own address. Four bits define the device (for example 1001 for the DS1831A thermometer chip) and three bits set an address unique to the device. Upon receiving the address from the master, each device makes a comparison to its own address. The device with the specified address then sends an acknowledge (ACK) signal back to the master. Now the master and slave may transmit information.

If the read/write bit transmitted with the address byte was a zero, the master will write to the device. To do this it sends a byte of data, known as a command byte, through the SDA line. After every byte of data the slave device must generate an ACK signal to acknowledge the byte was received. Only one bit of data is sent every SCL period meaning SDA may only change when SCL is low (the only exception being start and stop conditions). Including the ACK it takes nine SCL periods to send a byte of data on the bus. This continues until the master device sends a stop command signaling the bus is released (fig. 18).

If the read/write bit were instead a one, the master device will read from the specified device. In this instance the slave device will take control of the SDA line and send a command byte. This is followed by an ACK signal sent by the master

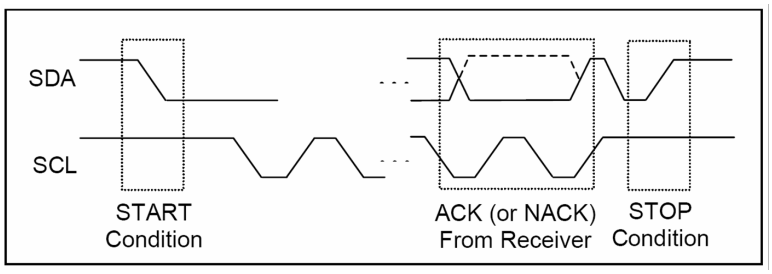

Figure 18: Start, stop, and ACK signals [8].

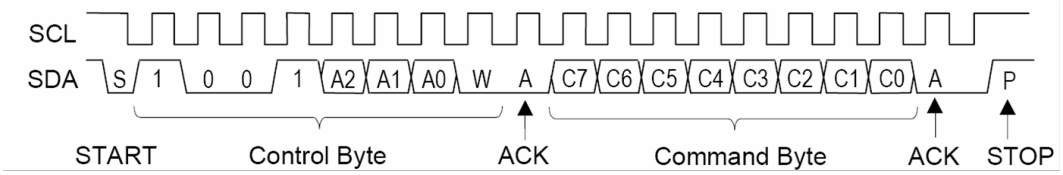

Figure 19: A sample exchange between the master and a slave device. The master device sends a start signal followed by the address byte. The slave device sends an acknowledge and the master device then sends a control byte. After the slave acknowledges the control byte the master sends a stop signal [10].

to the slave. This process continues until the master sends a "not acknowledge" command (NACK). The slave then releases control of the SDA line, and the master sends a stop command. When the bus is idle both the SDA and SCL lines are pulled high by a pull-up resistor. The I^2C has the capability to be multiplexed (i.e. to have several buses connected to one master device) for applications that require more than the available addresses on one bus.

4.3 I^2C Parallel Port Interface

During the testing and use of the vertical drift chambers it is important to have external and remote, far away from the radiation filled experimental hall, control of the front-end electronics. This is accomplished through use of the I^2C serial bus controlled by a master computer. An interface is needed to connect the computer

to the bus and for this purpose we have developed an I^2C parallel port interface. This interface has been designed to work specifically with a Linux kernel module intended to handle an I^2C bus. The kernel of an operating system is responsible for mediating between hardware and application software. In Linux separate modules can be plugged into the kernel to add functionality or behavior. This can be done without rebuilding the kernel or restarting the computer.

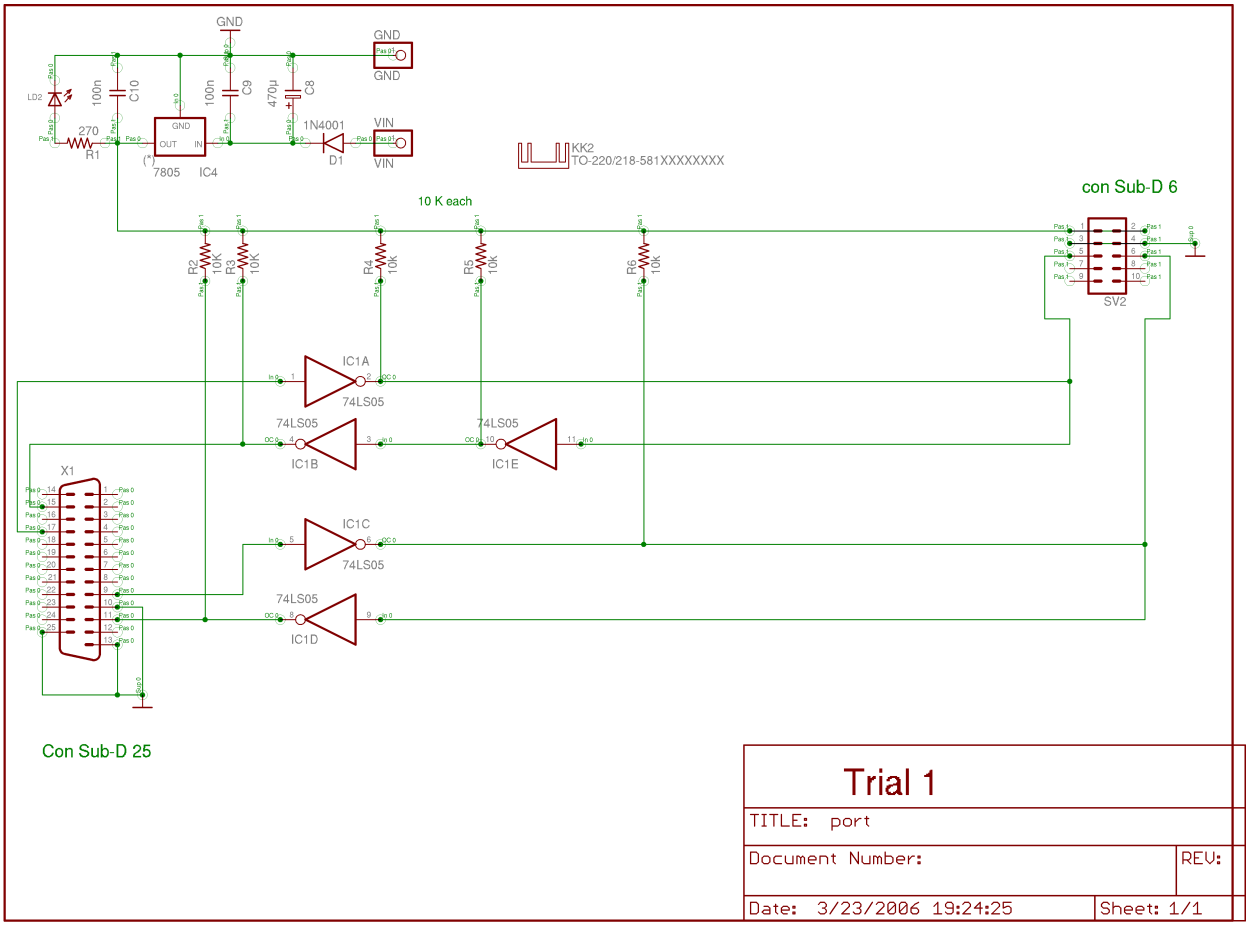

Figure 20: Schematic of the parallel port interface.

The parallel port interface is outfitted with a connector that plugs in to the 25 pin printer port on most personal computers. The lines designated by the Linux kernel module as SDA and SCL are routed directly from the parallel port to a 10 pin ribbon cable connector. This cable connector will connect all devices on the bus to

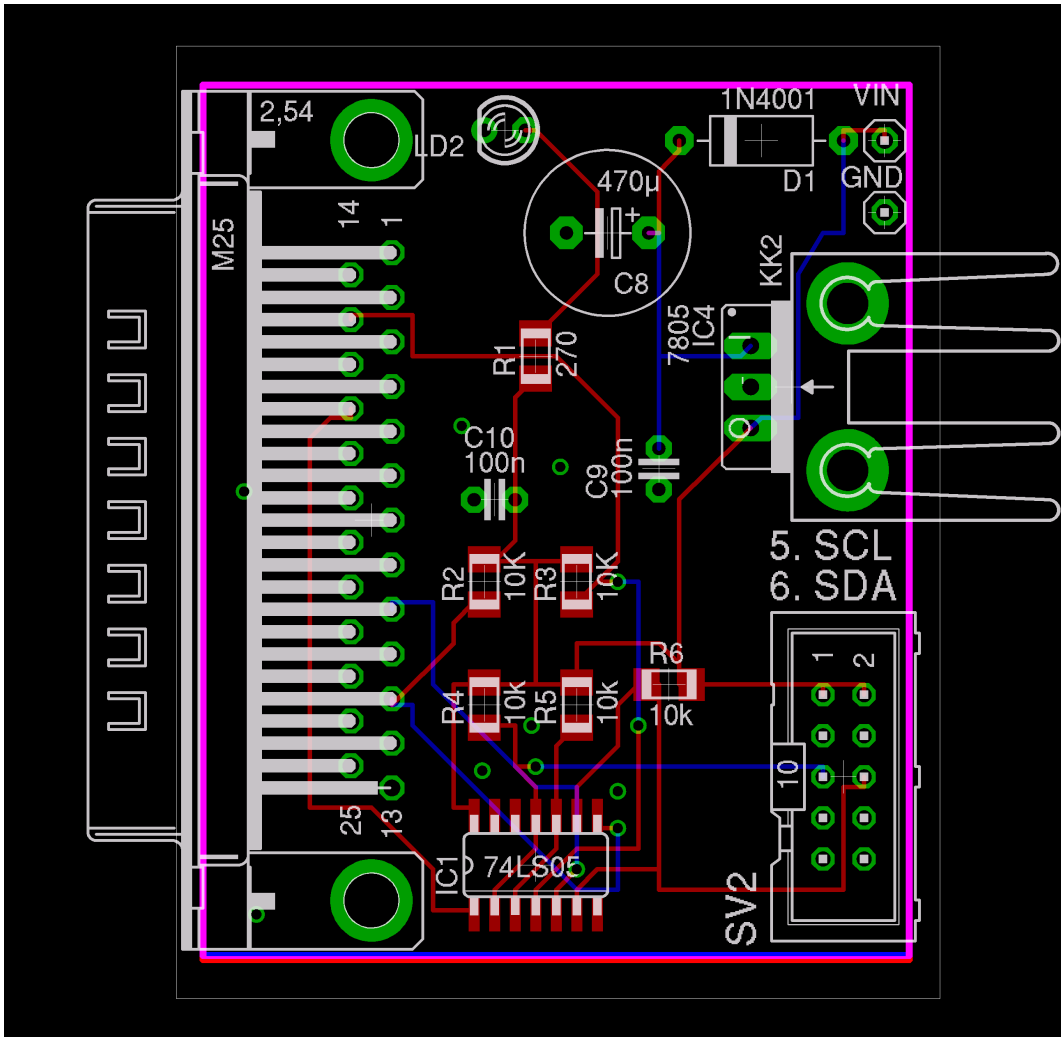

Figure 21: Board layout of the parallel port interface.

the computer. Both signal lines are tied to a 5 volt supply line by resistors. This is done so that SDA and SCL float high when no signal is applied to the lines. This is part of the I^2C protocol. The board is also equipped with a 5 volt power supply. Although the parallel port does provide a power supply, its output current (on the order of mA) is too small to drive multiple devices on the bus. The design of this power supply was taken from a similar interface card used in the BigBite experiment [9].

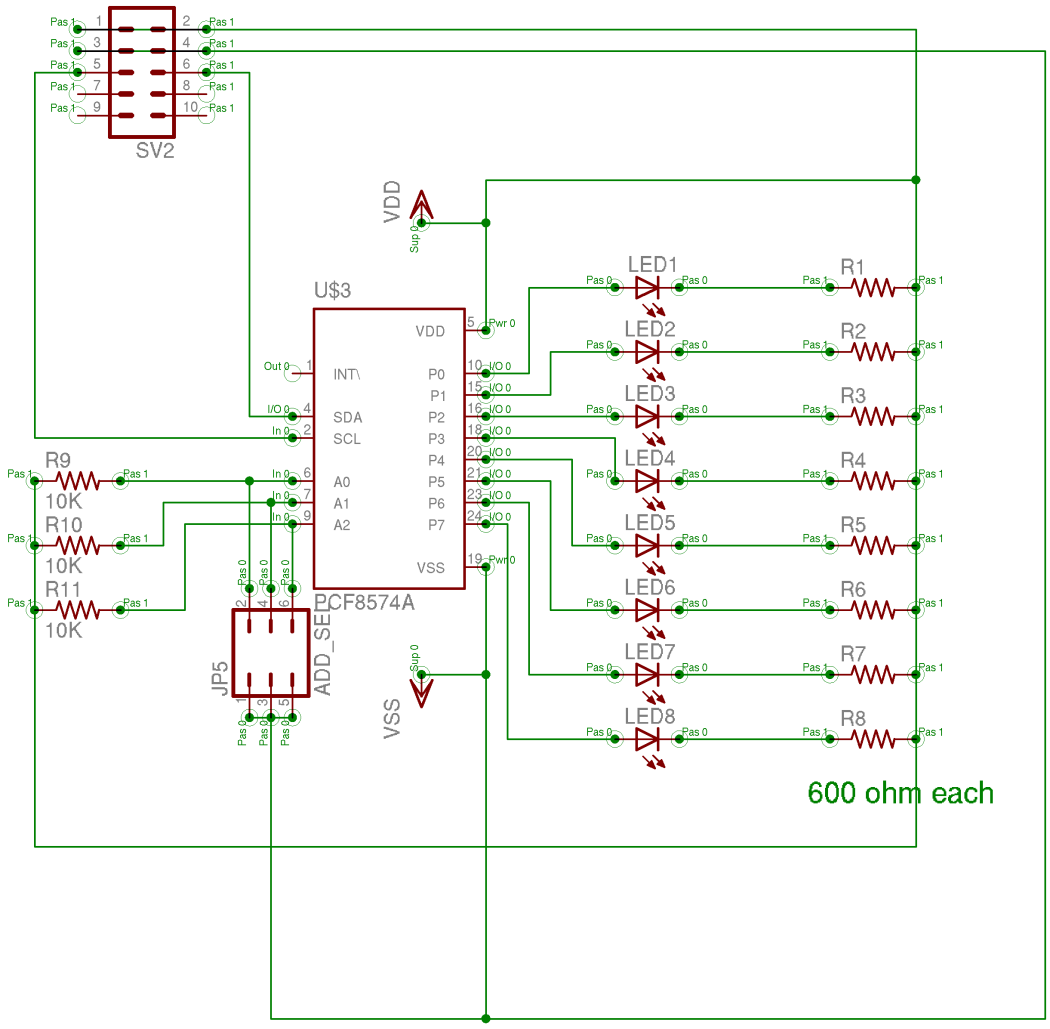

Figure 22: Schematic diagram of the channel enable/disable board.

4.4 Channel Enable/Disable Board

The channel enable/disable board is a prototype for the system that will enable and disable the individual channels of the MAD chip. This is an important feature for debugging the wire chambers, since some wires in the chamber may be faulty or some channels may ring, meaning they create internal feedback. In order to determine the channel or wire responsible for these problems it is necessary to have the capability to turn individual channels on and off. This is accomplished by using a PCF8574 chip produced by Phillips specifically for use on an I^2C bus. The chip itself has eight

input/output expansion ports, SDA and SCL lines, inputs for a power supply, three pins allowing a three bit address assignment, and an interrupt output (INT). This output allows the device to alert the master device that it is receiving input signals on its I/O ports while bypassing the bus. We will only be using the PCF8574 as an output device so this feature is not used on our boards.

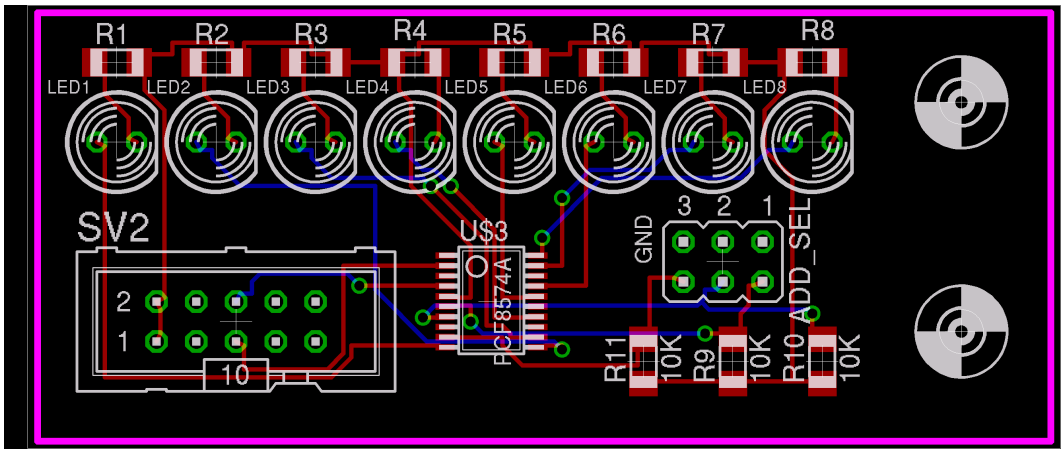

Figure 23: Board diagram of the channel enable/disbale board.

The board itself is outfitted with a 10-pin ribbon connector, allowing it to be attached to the serial bus either by direct connection to the parallel port interface or daisy-chained to another slave device on the bus. The lines carried by the ribbon cable, SDA, SCL, 5V, and GND, are routed directly to the PCF8574. Address selection is facilitated by a 6-pin header. Each address bit on the chip, A_0, A_1, and A_2, is connected to one pin on the header. Each of these pins can either be left open or jumped to the neighboring pin on the header, which is attached to ground. If the pin is left open the input to the address bit, which is attached by a resistor to 5 volts, will float high, producing a digital one. If instead the pin is jumped to the neighboring ground pin, the voltage will drop across the resistor and the address bit will register a digital zero. This is how one can select the address of the device.

For the prototype design all eight I/O pins of the PCF8574 are connected to light

emitting diodes (LEDs) to provide a visual confirmation that the device is working properly. In the final front-end electronics package these I/O pins will be connected to the analog enable pins of the MAD chip allowing the individual channels to be enabled or disabled.

4.5 Temperature Monitoring Board

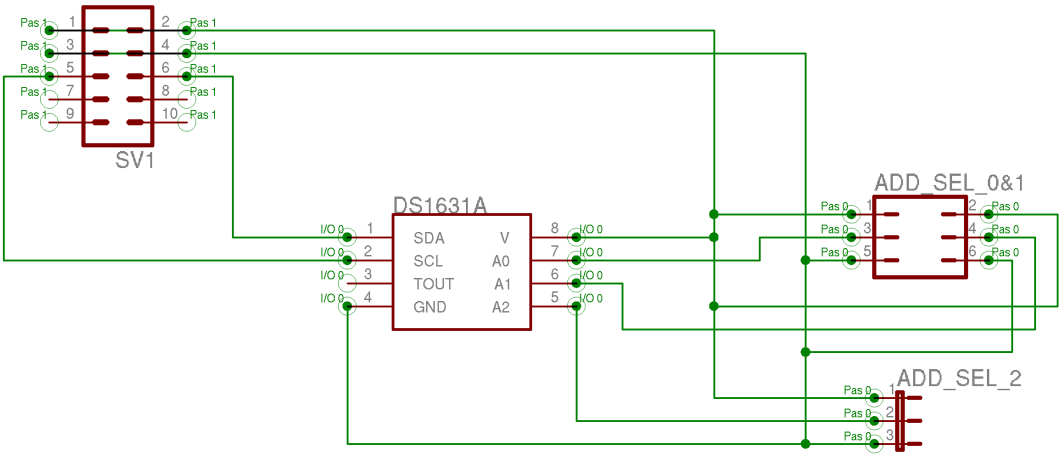

Figure 24: Schematic of the temperature monitoring board.

The MAD chip has two temperature outputs, one giving a constant analog temperature (T) and another (T_OUT) giving an analog temperature output only when enabled externally by a TTL high signal on the temperature enable pin (T_EN). It is important to know the temperature of the chip because the performance of analog electronics varies slightly over different temperature ranges. This change in the electronics manifests itself as an error in the timing of the digital output of the MAD chip. In order to correct for this, one must know how temperature affects the chip and then monitor the chip's temperature throughout the running of the experiment. On the final MAD chip boards the temperature output will be connected to an analog to digital converter (ADC) that is compatible with the I^2C serial bus and reads out

to the master device.

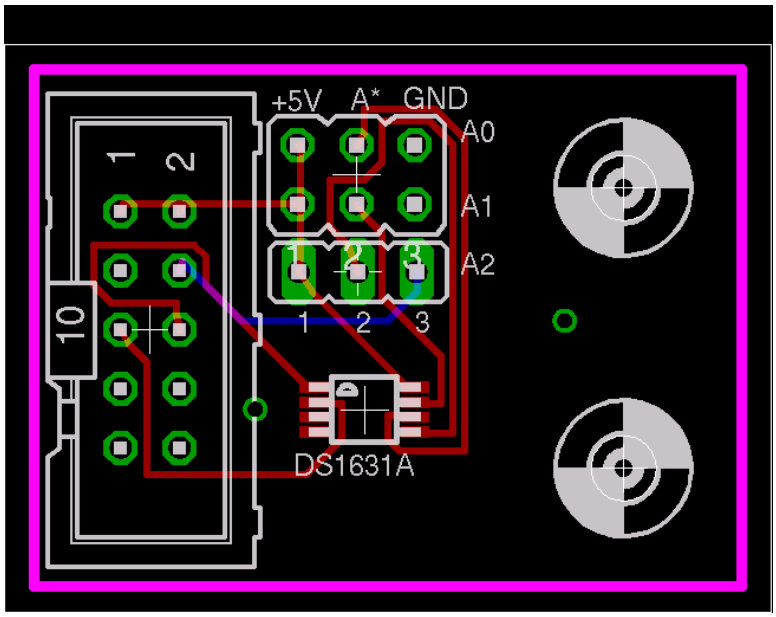

Figure 25: Board layout for the temperature monitoring board.

For the prototype electronics instead of using the temperature output of the complex MAD chip we have opted to use the DS1631, a high precision digital thermometer and thermostat chip produced by Dallas Semiconductor. The DS1631 is capable of measuring temperature using no other external components.

The DS1631 is powered by the 5V and GND lines originating on the parallel port interface card. The data line (SDA) and clock line (SCL) travel directly from the ribbon cable to the input pins on the chip. The chip has three address inputs allowing eight of these chips to be multidropped on the same bus. Each address pin is connected to a header pin. The header pin is then jumped to either ground, corresponding with a digital zero, or 5V, corresponding to digital one. In this way the device is assigned an address and can be called by the master to read out a temperature.

4.6 MAD Chip Test Board

The four channel amplifier discriminator MAD chip has several control options that we wish to investigate before using the chip with the drift chamber. This is done to determine the chip's characteristics and explore ways to get good timing from the chip. For this purpose I have designed a test board for use with the MAD chip. Design ideas were pooled from several sources [7], [6], [9].

The MAD chip is sensitive to external noise, so features are built into the board in an attempt to eliminate potential problems. The MAD chip requires two very stable low-noise power supplies, one for the analog portion of the chip and one for the digital portion of the chip. The board uses two linear voltage regulators from Micrel for this purpose. This power supply setup is identical to that used on the MAD chip boards developed for the BigBite experiment at Jefferson Lab [9]. Every voltage input on the MAD chip itself is connected to ground through a 100nF capacitor. This is to eliminate any high frequency noise carried on the power lines.

The test board allows four input signals attached with LEMO connectors. The output lines from the MAD chip run to a ten-pin ribbon cable connector for monitoring. Because the output is a low voltage differential signal (LVDS) each output from the chip has two lines which, in order to minimize noise, must run in parallel on the board. Each output is loaded by a 120 Ω resistor placed across the two lines.

Channels are enabled and disabled through the analog enable pins by Schmitt trigger NAND gates. Schmitt triggers are comparator circuits having the unique property of two voltage thresholds. Below one voltage threshold the input is considered low. Above the second higher threshold the voltage is considered high. Any voltage in between these thresholds causes the output to remain in its current state. In this way the Schmitt trigger eliminates the possibility of having a noisy signal oscillating right around a threshold value and rapidly switching the channels on and off. Using a Schmitt trigger for enabling channels has the further benefit of isolating the MAD

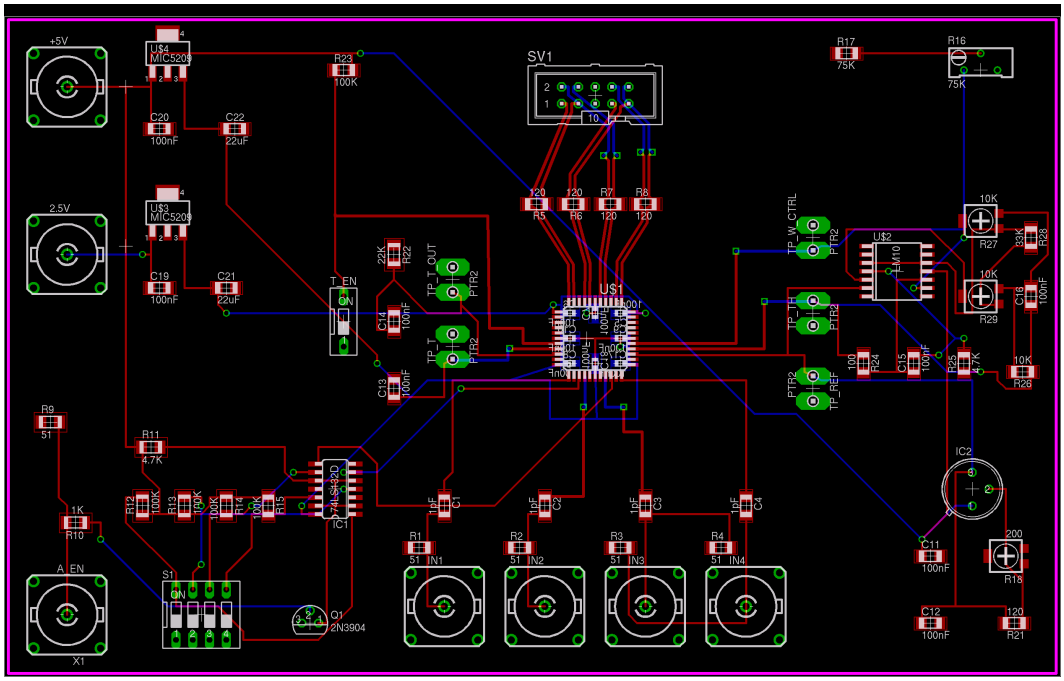

Figure 26: Board layout for the MAD chip test board.

chip from an an external TTL input. One input voltage for the Schmitt trigger is set using an analog switch on the board. Putting a channel's analog switch in the open position sets the voltage input to high, and a closed switch sets the voltage input to low. The second input of each Schmitt trigger is connected to a transistor which is in turn connected to an external LEMO input. When this external signal goes high, in this case greater than 0.6 V, the second input of the Schmitt trigger is attached to ground. When the external signal is low the second input of the Schmitt trigger floats high. Using this system one can manually set which channels they wish to be enabled and disabled and then remotely control the process through the external input.

The board is also equipped with electronics to control the threshold voltage (VTH), the quiescent baseline voltage (VREF), and the time width of the output (W_CTRL). The output time width is inversely proportional to the current sunk from the W_CTRL pin. This is done using a variable resistor attached to ground. By varying the resistance one can set different output pulse widths. The reference voltage is controlled

using the LM317, a 3 terminal adjustable voltage regulator made by National Semiconductor. The voltage regulator can be adjusted using a variable resistor attached to the adjust terminal of the chip. The output of the LM317 is routed to the VREF pin of the MAD chip. The threshold voltage (VTH) is set by an LM10 chip, an operational amplifier and voltage reference chip also made by National Semiconductor. The inverting input of the op-amp is the VREF voltage. This sets the minimum triggering voltage as the reference baseline voltage on which the amplified drift chamber signal is superimposed. This eliminates the possibility of triggering on a voltage lower than the drift chamber signal. The threshold voltage may be varied using a variable resistor. Test points are in place on W_CTRL, VREF, and VTH lines so they can be monitored at any time.

Temperature readout from the MAD chip is done by test points for both temperature output pins, T and T_OUT. The T pin has high output impedance (Z) and is simply connected to the test pads. The T_OUT pin has low output impedance and is loaded by a 22kΩ resistor to ground. Both outputs are connected to ground through a capacitor to eliminate any high frequency noise on the lines. The T_EN pin enables T_OUT and is controlled using a switch. When the switch is closed the pin is shorted to ground and T_OUT is disabled. When the switch is open T_EN floats high and T_OUT is enabled.

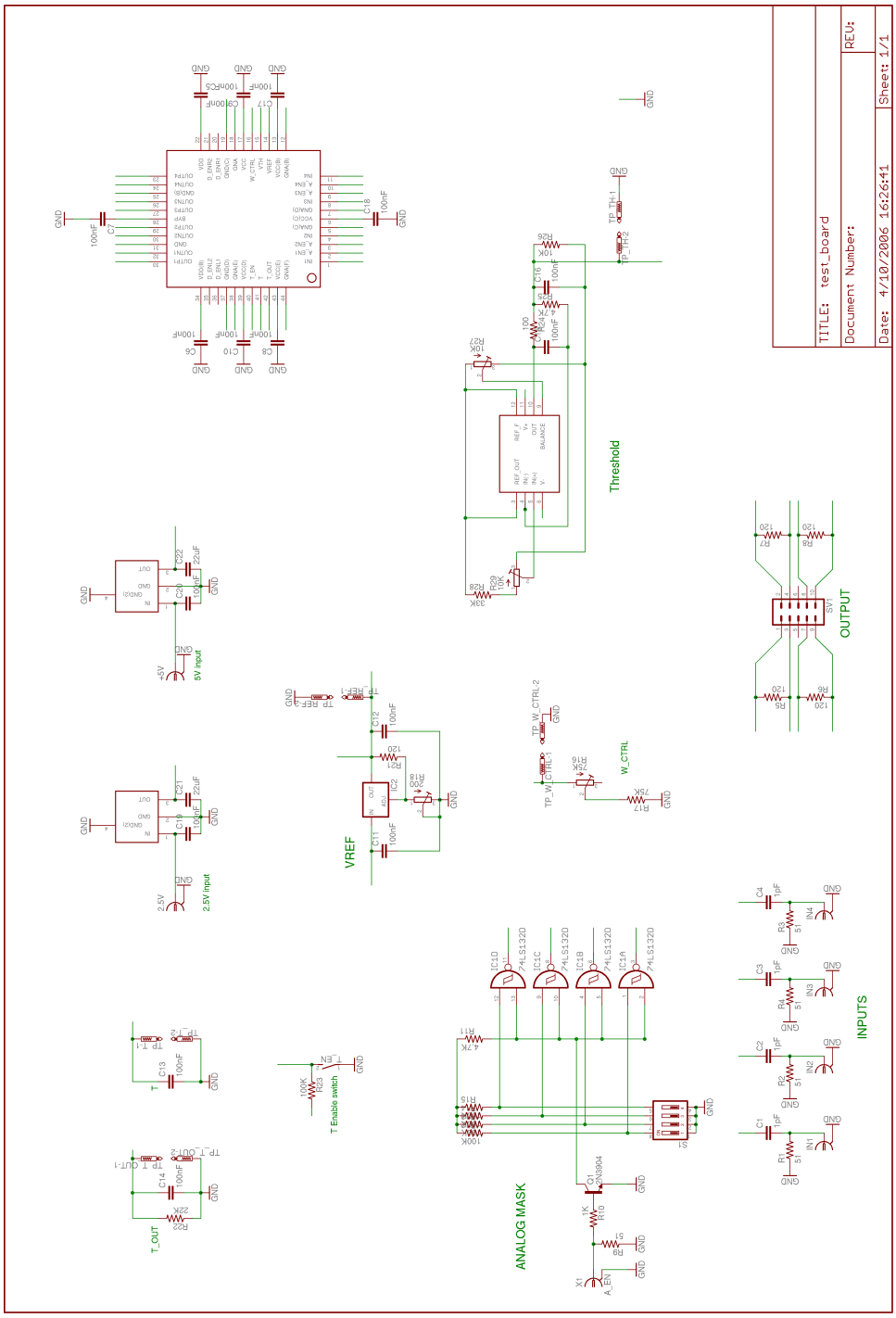

Figure 27: Schematic of MAD chip test board. For simplicity not all electrical connections are shown.

Once constructed, the MAD chip test board will allow the MAD chip to be tested and characterized under different conditions. It is important to have an understanding of the chip and its function before it is built into the final design for the front end electronics.

5 Conclusion

The vertical drift chambers for the Q_{weak} experiment at Jefferson Lab require a front-end electronics package to amplify and discriminate signals from wires in the drift chamber. In this thesis I have developed several printed circuit boards as prototypes for the electronics that will be used during the running of the experiment.

Much future work remains to be done before the Q_{weak} experiment is installed at Jefferson Lab in 2008. The PCBs discussed in this thesis have been ordered and printed by a company called Advanced Circuits. These boards must now be populated and tested. The MAD chip must also be tested in order to determine the best way to get good timing information from the chamber. Eventually designs for the final electronics package must be frozen and put into production.

References

[1] B.R. Martin and G. Shaw, "Particle Physics," 2^{nd} ed., Chichester: John Wiley and Sons, (1997).

[2] T.D. Lee and C.N. Yang, "Question of Parity Conservation in Weak Interactions," Phys. Rev. **104**, 254 (1956).

[3] C.S. Wu *et al.*, "Experimental Test of Parity Conservation in Beta Decay," Phys. Rev. **105**, (1957).

[4] S. Weinberg, "A Model of Leptons," Phys. Rev. **Lett. 19**, 1264-1266 (1967).

[5] D. Armstrong *et al.*, "The Q_{weak} Experiment: A search for new physics at the TeV scale via the measurement of the proton's weak charge," (http://www.jlab.org/qweak/), (2001).

[6] MAD Chip Description and Test Specifications, (http://dilbert.physics.wm.edu/elog/Construction/040713_154143/MAD-DESCRIPTION.pdf).

[7] P. Marzari, "Tesi di Laurea di Paola Marzari," (http://wwweda.pd.infn.it/cms/DTFB/electronics/frontend/homepage.html).

[8] DS1631 High Precision Digitial Thermometer and Thermostat data sheet, (http://pdfserv.maxim-ic.com/en/ds/DS1631-DS1731.pdf/).

[9] C. Cuevas, private communication.

[10] A. Wolf, "I2C Bus Technical Overview and Frequently Asked Questions," (http://www.esacademy.com/faq/i2c/).

[11] J. Erler *et al.*, "The Weak Charge of the Proton and New Physics," (2003).

[12] G. Garvey and S. Seestrom, "Parity Violation in Nuclear Physics: signature of the weak force," Los Alamos Science **21**, (1993).